Neutron-skin and proton-skin formations in exotic nuclei far from stability

N. Fukunishi,[1,2] T. Otsuka,[1,3] and I. Tanihata[2]
[1]*Department of Physics, University of Tokyo, Hongo, Tokyo 113, Japan*
[2]*RIKEN, 2-1 Hirosawa, Wako, Saitama 351-01, Japan*
[3]*Institute for Nuclear Theory, University of Washington, Seattle, Washington 98105*
(Received 23 February 1993)

The neutron skin is studied in terms of the Hartree-Fock calculation, and its new definition is presented and discussed. It turns out that the neutron skin is closely related to how far the nucleus is away from the β stability line, but not directly to the number of excess neutrons. Related properties of Hartree-Fock calculations for unstable nuclei are discussed. Novel features associated with the neutron skin are suggested, for instance, neutron avalanche in reactions involving a nucleus with the neutron skin. The formation of the proton skin is shown to be rather difficult.

PACS number(s): 21.10.−k, 21.10.Ft, 21.10.Gv, 21.60.Jz

I. INTRODUCTION

The neutron skin of the nucleus has been one of the central issues of nuclear structure [1,2]. The definition and presence of the neutron skin, however, have remained open problems for decades. It is only recently that thick neutron skins have been seen experimentally, although only quite light nuclei such as ^{6}He and ^{8}He were investigated [3]. In this paper, we present results of Hartree-Fock calculations [4–6] with standard Skyrme interactions (SIII and SGII) [6,7] for several chains of isotopes. We introduce a definition of the neutron skin, which suggests that the neutron skin does not appear in nuclei near the β stability line, but a neutron skin with more than ten neutrons can be formed in nuclei far from the stability line. The proton skin is discussed also, although its formation appears to be rather difficult.

II. HARTREE-FOCK CALCULATION AND RESULTING DENSITIES

We solve the Hartree-Fock equation with the Skyrme(-type) interactions for a number of nuclei with various values of the neutron number (N) and the proton number (Z). The Hartree-Fock equation can be extended for open-shell nuclei if the occupation number of each orbit is given as input [5,6]. We simply take advantage of this prescription by combining it to the BCS calculation of the occupation probabilities of the valence-shell orbits. Such an extended Hartree-Fock calculation implies, as is well known, a variation of the energy for a certain linear combination of various states. To be more precise, various configurations are taken with the occupation probabilities which are evaluated by the BCS in the present calculation, and a particular linear combination belonging to each configuration is considered [5,6]. Although this linear combination includes not only the ground state but also other states, uncertainties due to this technical problem should be rather irrelevant to our major results of this paper, because we restrict ourselves to bulk properties such as densities and radii which are rather common along those states and are not very sensitive to details of the structure. The pairing-force strength is assumed as $G=30/A$ MeV for protons and $G=20/A$ MeV for neutrons where A means the mass number. Although this pairing-force strength for protons may be stronger than the usual value, the resulting pairing gap Δ is reasonable compared to the empirical one $\Delta=12A^{-1/2}$ MeV [8]. The Coulomb interaction is included with the exchange term in the Slater approximation. In this paper, for simplicity, we focus on the Hartree-Fock calculation for the spherical equilibrium [6]. A similar theoretical calculation has been done in terms of a relativistic mean-field model for neutron-rich nuclei [3].

We shall now discuss Cs isotopes ($Z=55$) as an example. Figure 1(a) shows the proton and neutron densities of ^{133}Cs as a function of the distance r from the center of the nucleus. The nucleus ^{133}Cs is stable with 100% natural abundance. Since $Z=55$ and $N=78$, the neutron density, denoted by $\rho_n(r)$, is larger than the proton density $\rho_p(r)$ by a factor $\sim N/Z$ over the whole range of r. On

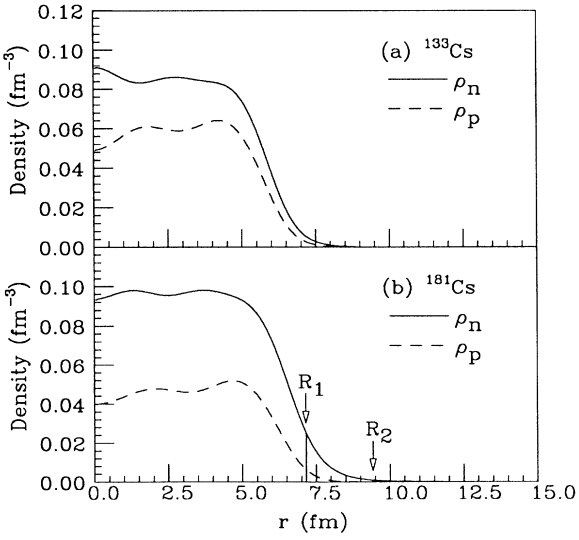

FIG. 1. Neutron (solid line) and proton (dashed line) densities for (a) ^{133}Cs and (b) ^{181}Cs.

the other hand, the proton root-mean-square radius R_p is quite close to the neutron radius R_n. A similar situation is confirmed also in ^{208}Pb, for instance.

Figure 1(b) shows the density of ^{181}Cs where $N=126$. One sees that $\rho_n(r)/\rho_p(r) \sim 2.0$ in the interior region. This value is not far away from $N/Z=2.3$, whereas $\rho_n(r)/\rho_p(r)$ becomes much larger for $r>7$ fm. In other words, the nucleus ^{181}Cs seems to contain some features of the neutron skin to be discussed below.

III. DEFINITION OF NEUTRON SKIN

The ratio $\rho_n(r)/\rho_p(r)$ is about N/Z in the interior region of basically all nuclei. In some nuclei, the ratio can somewhat exceed N/Z around the nuclear surface. Such deviations, however, can be ascribed to accidental fluctuations due to shell effects, etc., in many cases, and then do not reflect any characteristic physical meanings. In order to distinguish, at least theoretically, the neutron skin from such less interesting fluctuation effects, we introduce a definition of the neutron skin in terms of the following three criteria.

(1) In the neutron skin,

$$\rho_n(r)/\rho_p(r) > \xi_1 \tag{1}$$

should hold with a large value of ξ_1. Since $\rho_n(r)/\rho_p(r) \sim N/Z$ in the interior region, ξ_1 should be larger than N/Z. In practice, we take $\xi_1=4$ in this paper. The radius R_1 is determined by the condition $\rho_n(R_1)/\rho_p(R_1)=\xi_1$. Since $\rho_p(r)$ decreases quickly near and beyond $r \sim R_1$, R_1 does not strongly depend on the adopted value of ξ_1 if it is sufficiently larger than N/Z. The value of R_1 in Fig. 1(b) is 7.15 fm.

(2) The neutron skin is introduced as a layer of neutrons containing a sizable number of neutrons. Therefore, the neutron density in the skin should not be too dilute. The following inequality is then imposed in the skin,

$$\rho_n(r) > \xi_2 \rho_n(0) , \tag{2}$$

where $\rho_n(0)$ is the neutron density at the center of the nucleus. Equations (1) and (2) mean that the skin stretches from $r=R_1$ up to $r=R_2$, where R_2 is determined by $\rho_n(R_2)=\xi_2\rho_n(0)$. The value of ξ_2 is taken to be $\frac{1}{100}$ in this paper, so that the neutron skin can be discriminated from the neutron halo which stretches outwards from around the radius with $\rho_n(r) \sim \frac{1}{100}\rho_n(0)$ as discussed later [9]. The condition in Eq. (2) is important to measure the thickness of the skin, but is rather irrelevant for the number of neutrons in the skin because of the low density in the outer part. The value of R_2 in Fig. 1(b) is 9.43 fm.

(3) The difference $\delta R \equiv R_2 - R_1$ is referred to as the skin thickness. Some nuclei, for example, ^{133}Cs, have R_1 greater than R_2. In this case, the skin thickness is defined as $\delta R=0$. A nucleus is defined to have a neutron skin if the following inequality is fulfilled:

$$\delta R \geq \xi_3 , \tag{3}$$

where ξ_3 is an appropriately chosen constant. The value of ξ_3 is taken to be 1 fm presently, because 1 fm is about equal to the range of the nuclear force and $\delta R > 1$ fm means that there is a sizable amount of neutrons separated from most of the protons by a distance larger than the range of the nuclear force. We summarize three criteria mentioned above in Table I. If one applies these three criteria, it turns out that ^{133}Cs has no skin, whereas ^{181}Cs does. In fact, for ^{181}Cs, $R_1=7.15$ fm and $R_2=9.43$ fm, resulting in $\delta R=2.27$ fm. Note that $R_1=8.67$ fm and $R_2=8.05$ fm for ^{133}Cs, which means that $\rho_n(r)$ damps quickly below ξ_2, before $\rho_n(r)/\rho_p(r)$ increases above ξ_1. As stated earlier, we set $\delta R=0$ in this case. If we apply these criteria, it turns out that ^{208}Pb has no neutron skin either.

TABLE I. Criteria for the neutron skin.

Condition	Adopted value	Remark
(1) $\rho_n(r)/\rho_p(r) > \xi_1$	$\xi_1=4$	Inner boundary (R_1)
(2) $\rho_n(r) > \xi_2\rho_n(0)$	$\xi_2=\frac{1}{100}$	Outer boundary (R_2)
(3) $\delta R \geq \xi_3$	$\xi_3=1$ fm	$\delta R = R_2 - R_1$

Figures 2(a) and 2(b) show, as a function of N, the skin thickness and the number of neutrons in the skin for the Cs isotopes. The skin thickness remains zero up to $N=84$, and then increases continuously. The number of skin neutrons also remains zero up to $N=84$, and then increases together with the skin thickness. The neutron number in the skin reaches about twelve for $N=126$. In other words, about 10% of the neutrons in ^{181}Cs are in the skin.

Figure 2 suggests a strong correlation between the neutron skin and the stability of the nucleus. Protons and neutrons interact strongly so as to gain a large binding energy, which in fact becomes largest around the β stability line within an isobar chain. Since the nuclear force is of short range, the proton distribution should be well overlapped with the neutron distribution in nuclei near the β stability line. This results in approximately equal

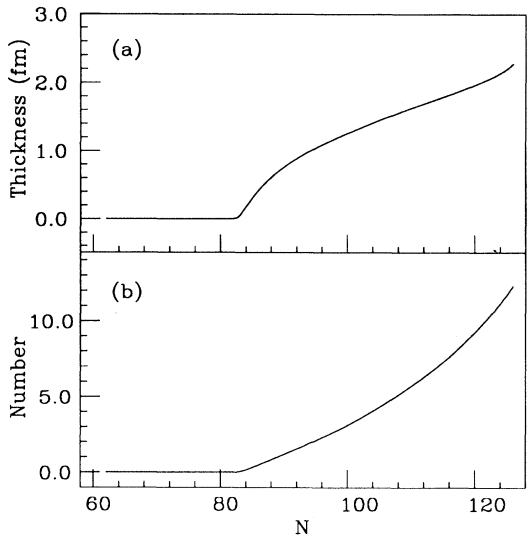

FIG. 2. (a) Skin thickness and (b) the number of neutrons in the skin for Cs isotopes as a function of the neutron number N. The SIII interaction is used.

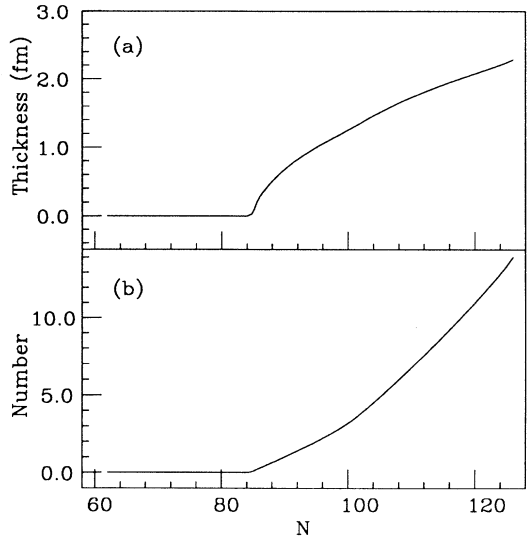

FIG. 3. See the caption of Fig. 2. The SGII interaction is used.

mean-square radii of protons and neutrons. The root-mean-square radii R_p and R_n of the stable isotope ^{133}Cs are, for instance, $R_p = 4.80$ fm and $R_n = 4.90$ fm, which are indeed very close to each other. On the other hand, for ^{181}Cs, the above argument no longer holds, and one obtains $R_p = 5.15$ fm and $R_n = 5.56$ fm. The origin of this difference will be discussed in the next section.

Other Skyrme interactions produce basically the same results as in Fig. 2. As an example, the result obtained from the SGII [7] interaction is shown in Fig. 3. The skin thickness and the number of neutrons in the skin show nearly identical values to those in Fig. 2, while, for $N \sim 126$, the values are somewhat higher in Fig. 3 than in Fig. 2.

IV. NEUTRON-SKIN FORMATION MECHANISM AND MEAN POTENTIAL

We shall discuss in this section in what mechanism the neutron skin is formed. The present calculations show that the following three mechanisms work for basically all nuclei including those far from stability (see Fig. 1): (1) the proton and neutron densities remain approximately uniform in the interior region, (ii) the radius of such uniform interior part of protons has a similar value to that of neutrons, and (iii) the sum of the proton and neutron densities, i.e., the total (mass) density is about 0.15 fm^{-3}. Because of these mechanisms, as the neutron number increases from the β stability line, the proton density in the interior decreases, whereas the neutron density increases, so that the total (mass) density is kept about the same (~ 0.15 fm^{-3}). Both the proton and neutron mean-square radii are then increased gradually. The proton-neutron interaction is stronger than the proton-proton or neutron-neutron interaction. Therefore, if the neutron density increases, the mean potential for protons becomes deeper. Consequently, protons are more deeply bound as seen already for ^{48}Ca in Ref. [4]. This gives rise to stronger damping of the proton density in the exterior and an increase of the number of bound orbits. We emphasize once more that the proton density goes down as the neutron number increases (within a given isotope chain).

We now turn to the potential for neutrons. As going away from the β stability line with more neutrons, the proton density decreases, and then the potential for neutrons becomes shallower because of the strong proton-neutron interaction. As more neutrons are added to the nucleus and the potential becomes shallower, the neutron Fermi energy goes up and many neutrons are bound more loosely. In this situation, the energy of the total system can be lowered by expanding the neutron density distribution with its weakened damping towards the exterior, because, by this expansion, the kinetic energy is lowered but only a relatively small binding energy is lost owing to the shallow potential. This implies that the neutron density distribution is stretched out. Thus, the shape proportionality between the proton and neutron densities are broken in the outer region of nuclei with $N \gg Z$, and thus the neutron skin emerges. This mechanism of the neutron-skin formation is a general one, and indicates that the neutron skin should occur rather independently of minor details of calculations. For instance, Fig. 3 indicates that the results remain almost unchanged when another Skyrme interaction SGII [7] is used.

We shall now look at the Hartree-Fock potentials actually obtained. Figures 4(a) and 4(b) show the Hartree-Fock potentials U_p and U_n (see Eq. (22a) of Ref. [4]) for protons and neutrons, respectively, for ^{133}Cs (^{181}Cs) with the SIII interaction. In the case of ^{133}Cs, which is stable,

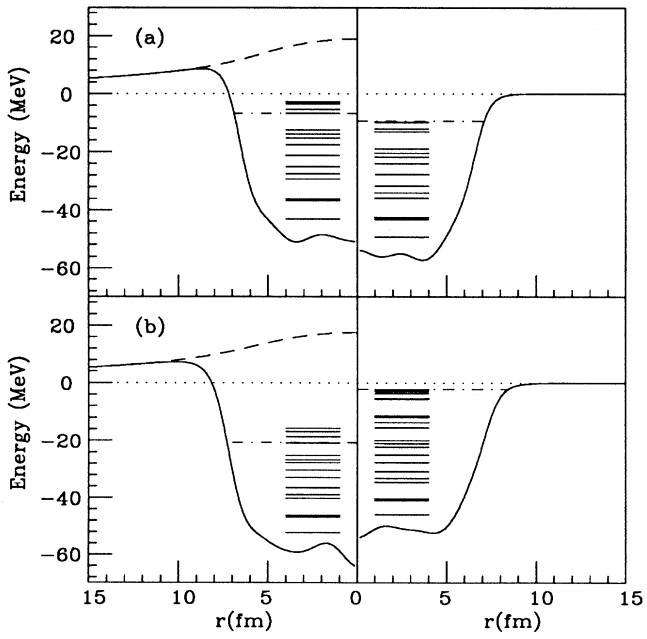

FIG. 4. Mean-field quantities for protons (left) and neutrons (right) in (a) ^{133}Cs and (b) ^{181}Cs. Solid lines indicate Hartree-Fock potentials which include the Coulomb term (dashed line) for protons. Fermi energy (dot-dashed bar) and Hartree-Fock single-particle energies around and below it (shorter bars) are shown.

U_p and U_n have similar shapes except for the Coulomb contribution. The single-particle energies and Fermi energies are also indicated in Figs. 4(a) and 4(b). One finds that the proton Fermi energy $\epsilon_p^{(F)}$ is very close to the neutron one $\epsilon_n^{(F)}$ in ^{133}Cs [see Fig. 4(a)]. The proton and neutron Fermi energies should be close to each other in β stable nuclei, otherwise β decays should take place.

The situation differs drastically in ^{181}Cs which is far from the stability line. The shape of U_n is different from that of U_p, in particular on the surface, where the slope of U_n is less steep. For a more precise comparison, the potentials are compared directly between ^{133}Cs and ^{181}Cs in Fig. 5. It can be seen, for instance, that, at the radial point where the potential is half of its central value, the slope of U_n for ^{181}Cs is about 80% of the value for ^{133}Cs. The proton potential U_p becomes deeper by the reason discussed earlier, whereas the slope of U_p on the surface remains rather unchanged. The gradual slope of U_n for ^{181}Cs on the surface is produced primarily by the neutrons in the neutron skin, because the proton density is damped there very quickly. The most prominent difference seen in Figs. 4(a) and 4(b) is that $\epsilon_p^{(F)}$ and $\epsilon_n^{(F)}$ are no longer close to each other for ^{181}Cs. Note that $\epsilon_p^{(F)}$ is pushed down compared to ^{133}Cs. The potentials obtained from the SGII interaction shows very similar features to those in Figs. 4 and 5, whereas the SGII interaction produces slightly stronger binding for the neutron potential around the surface, favoring the neutron-skin formation.

Here, we proceed to the study of the effective mass. The following expression holds for the SIII interaction:

$$\frac{\hbar^2}{2m_q^*(r)} = \frac{\hbar^2}{2m} + \frac{t_1+t_2}{4}\rho + \frac{t_2-t_1}{8}\rho_q \ , \tag{4}$$

where $m_q^*(r)$ is the effective mass and m means the bare nucleon mass. q denotes the proton or neutron. t_1 and t_2 are the Skyrme parameters. Thus, the isospin dependence of the effective mass is determined by the last term on the right-hand side of Eq. (4). The effective masses of the ^{133}Cs and ^{181}Cs are illustrated in Figs. 6(a) and 6(b), using the SIII and SGII interactions, respectively. We can find that the effective mass of neutrons in the nuclear interior becomes larger as the neutron number increases. On the other hand, the effective mass of protons becomes smaller for ^{181}Cs. The larger effective mass of neutrons in ^{181}Cs partially compensates for the shallower mean potential of neutrons in neutron-rich isotopes, because the wave function is actually determined by the product of the effective mass and the mean potential:

$$\frac{2m_q^*(r)}{\hbar^2} U_q(r) \ .$$

However, the isospin dependence of the effective mass is weaker than that of the mean potential when we use the SIII and SGII interactions, which give the appropriate single-particle spectra and the surface diffuseness. (The parameters t_1 and t_2 are strongly related to the single-particle spectra and the surface diffuseness.) Using the SIII interaction, the averaged depth of the neutron mean

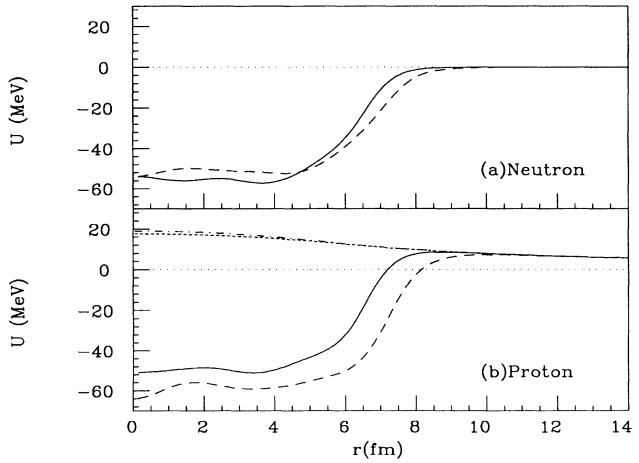

FIG. 5. Hartree-Fock mean potentials for (a) neutrons and (b) protons. The nuclei ^{133}Cs (solid lines) and ^{181}Cs (dashed lines) are compared directly. The potentials are the same as those shown in Fig. 4.

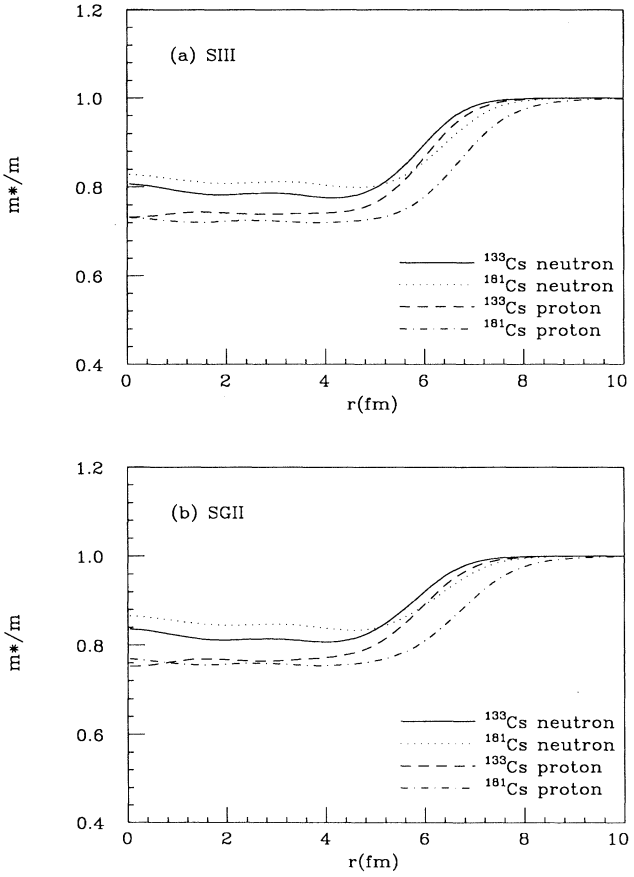

FIG. 6. Hartree-Fock effective masses using (a) the SIII and (b) the SGII interactions. The ratio of the effective mass to the bare nucleon mass $[m^*(r)/m]$ is shown. The neutron effective masses are shown using the solid line (^{133}Cs) and the dotted line (^{181}Cs). The proton effective masses are also shown using the dashed line (^{133}Cs) and the dot-dashed line (^{181}Cs).

potential in the nuclear interior ($r < 4$ fm) is 8.9% smaller for ^{181}Cs than for ^{133}Cs. On the other hand, the averaged value of the effective mass becomes 3.4% larger. Thus, the potential change exceeds the change of the effective mass, and we need not modify qualitatively the discussion for the formation of the neutron skin. We must mention that the isospin dependence of the effective mass is not understood directly by experiment and further investigation is needed both theoretically and experimentally.

We will discuss the energy-dependent equivalent local potential for these neutron-rich nuclei. In the case of the Skyrme Hartree-Fock (HF) approximation, the energy-dependent equivalent local potential, which gives the same phase shift as the original HF equation, was introduced by Dover and van Giai [10]. Using the HF mean potential $U_q(r)$ [see Eq. (22a) of Ref. [4]] and the effective mass $m_q^*(r)$, the central part of the energy-dependent equivalent local potential is defined as follows:

$$V_q^{\rm cent}(r,E)=\frac{m_q^*(r)}{m}\left[U_q(r)+\frac{1}{r}\frac{d}{dr}\frac{\hbar^2}{2m_q^*(r)}+\frac{1}{2}\frac{d^2}{dr^2}\frac{\hbar^2}{2m_q^*(r)}-\frac{m_q^*(r)}{2\hbar^2}\left[\frac{d}{dr}\frac{\hbar^2}{2m_q^*(r)}\right]^2\right]+\left[1-\frac{m_q^*(r)}{m}\right]E\ . \tag{5}$$

The average potential and the symmetry potential are introduced following Ref. [10] as

$$V_{\rm av}^{\rm cent}(r,E)=\tfrac{1}{2}[V_n^{\rm cent}(r,E)+\tilde{V}_p^{\rm cent}(r,E)]\ , \tag{6}$$

$$V_{\rm sym}^{\rm cent}(r,E)=\tfrac{1}{2}[V_n^{\rm cent}(r,E)-\tilde{V}_p^{\rm cent}(r,E)]\ , \tag{7}$$

where $\tilde{V}_p^{\rm cent}$ is the nuclear part of the equivalent local potential where the Coulomb potential has been removed. We restrict ourselves to the energy-independent part of the equivalent local potential in this paper. The average potential and the symmetry potential for various Cs isotopes are illustrated in Figs. 7(a) and 7(b), respectively. The average potential changes systematically as the neutron number increases. These can be fitted well by the simple Woods-Saxon form,

$$V_{\rm av}^{\rm cent}(r)\approx\frac{V_0}{1+\exp[(r-R)/a]}\ , \tag{8}$$

$$R=r_0A^{1/3}\ , \tag{9}$$

where A denotes the mass number. We find that the strength parameter V_0 is almost constant for all Cs isotopes, namely, $V_0=-47.4\pm0.6$ MeV. The radius parameter r_0 also remains constant, $r_0=1.27$ fm. These results are very similar to the discussion for stable nuclei [10]. On the other hand, we find the new characteristic behavior about the diffuseness parameter a for nuclei with the neutron skin. The diffuseness parameter is shown in Fig. 8 as a function of the neutron number. The diffuseness parameter takes almost the same value, $a=0.50$ fm, for stable nuclei, for example, ^{90}Zr, ^{120}Sn, ^{133}Cs, and ^{208}Pb. As the neutron number goes away from the β stability line, the diffuseness parameter also increases showing strong correlation to the skin thickness. The diffuseness parameter for ^{181}Cs is 12% larger than that of ^{133}Cs. The $\rho\nabla^2\rho$ term in $U_q(r)$ plays an important role in this behavior. The symmetry potential, which sharply reflects the excess density $(\rho_n-\rho_p)$ as discussed by Dover and Giai [10], changes remarkably as the neutron number increases. They are shown in Fig. 7(b). In the neutron-rich isotopes, the symmetry potential expands outwards and becomes larger. In ^{181}Cs, the symmetry potential works so as to make the proton potential steeper and the neutron potential less steep. The differences of the surface slope between the proton and the neutron mean potentials are correlated sensitively with the shape and the peak position of the symmetry potential. Note that the average potential becomes less steep in the neutron-rich nuclei, whereas the symmetry potential shows a more magnificent peak.

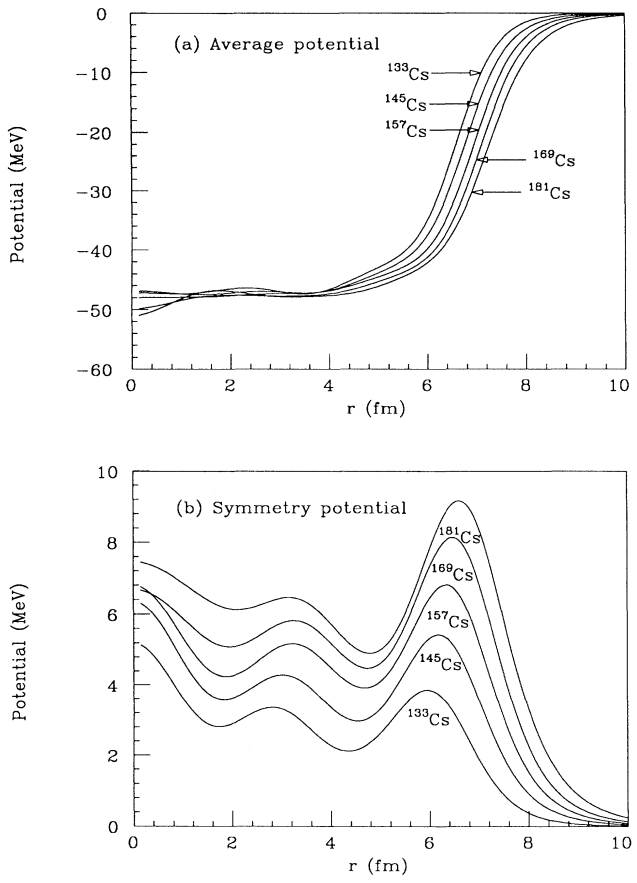

FIG. 7. Equivalent local potential for vairous Cs isotopes. The energy independent, central part of (a) the average potential and (b) the symmetry potential are calculated using the SIII interaction.

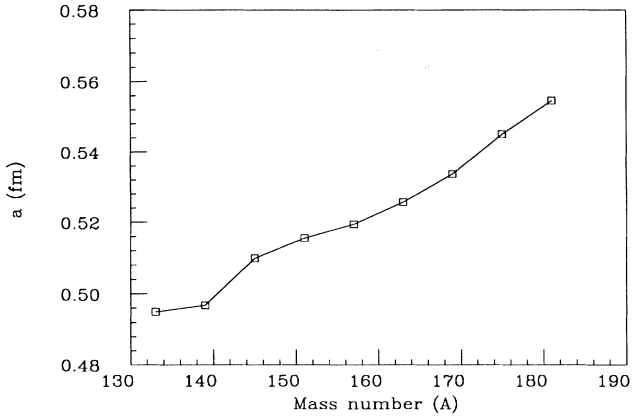

FIG. 8. The diffuseness parameter of the average potential for various Cs isotopes as a function of the mass number. The diffuseness parameter is determined using the χ-square fitting for the average potential shown in Fig. 7(a).

V. CALCULATIONS FOR *sd*-SHELL NUCLEI

Similar calculations can be done for a variety of nuclei. In Fig. 9, the skin thickness and the number of skin neutrons are shown for Na, Mg, and Al isotopes as a function of N. We find that the neutron skin is formed also in light nuclei if the β stability line is sufficiently far.

VI. ROOT-MEAN-SQUARE RADIUS

The neutron skin has been discussed in some cases in terms of the ratio $2(R_n-R_p)/(R_n+R_p)$, where R_n (R_p) denotes the neutron (proton) mean-square radius. This ratio is reported experimentally to be $0.7^{+2.3}_{-0.7}\%$, $4.1^{+2.1}_{-2.5}\%$, and $3.0\pm1.3\%$ for ^{116,124}Sn and ^{208}Pb, respectively [1]. The present calculation applied to these nuclei shows the corresponding values, 1.59%, 2.85%, and 2.24%, which are all within error bars and show variation consistent with experiment. These nuclei do not have the neutron skin according to the present criteria shown in Table I. The calculated ratio reaches 7.7% for ^{181}Cs.

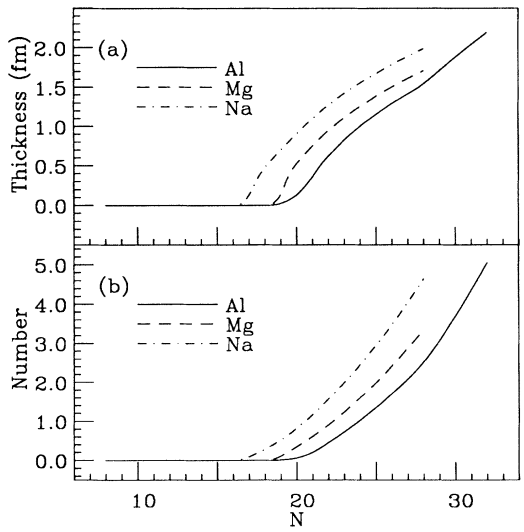

FIG. 9. (a) Skin thickness and (b) the number of neutrons in the skin for Na (dot-dashed line), Mg (dashed line), and Al (solid line) isotopes as a function of the neutron number N.

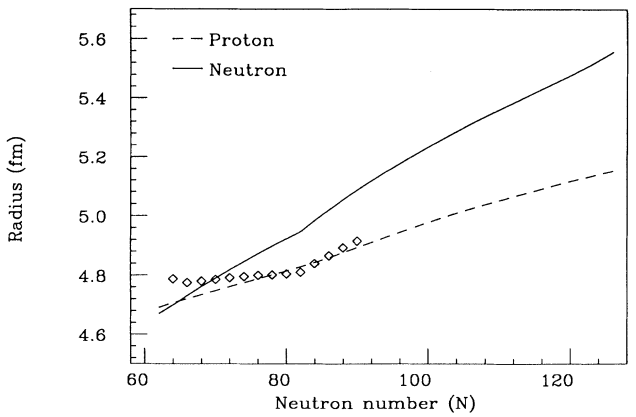

FIG. 10. rms radii for neutrons (solid line) and protons (dashed line) of Cs isotopes. Experimental rms charge radius is included (points) with adjustment at ^{133}Cs.

Figure 10 shows the rms radii for Cs isotopes. The proton radius is compared with the observed root-mean-square charge radius compiled in Ref. [11]. Note that differences from ^{133}Cs can be measured and the observed "radius" is adjusted to the calculated value at ^{133}Cs. The difference between the proton radius and charge radius due to the finite size of a proton is neglected in Fig. 10, because this difference is considered to remain nearly constant as a function of the neutron number and therefore does not affect the comparison in Fig. 10 so sensitively. The center-of-mass correction in the calculation is neglected similarly. One finds a fairly good agreement between the present calculation and the experiment for $N \geq 78$. Although the agreement is not good for smaller N, the present study concerns nuclei with larger N.

VII. PROTON SKIN

The proton skin can be discussed in a similar way to the neutron skin. Figure 11 shows the proton and neutron densities of ^{21}Al and ^{27}Al. The proton density

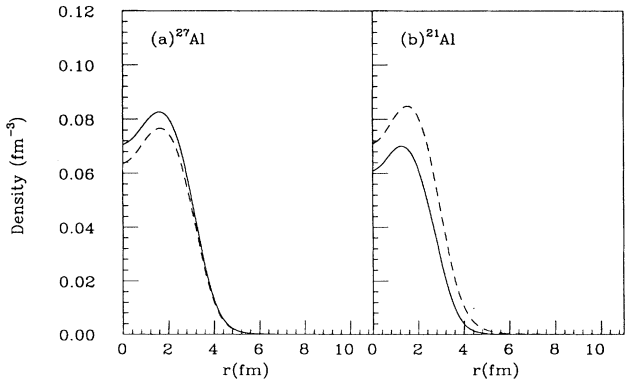

FIG. 11. Neutron (solid line) and proton (dashed line) densities for (a) ^{27}Al and (b) ^{21}Al.

profile does not change between these two nuclei, whereas the neutron density distribution is squeezed in ^{21}Al. For an unstable nucleus ^{21}Al, δR defined in Eq. (3) becomes 0.84 fm for protons. This value is slightly less than the criterion (3) in Table I, but indicates a situation close to the proton skin formation.

In contrast, the proton skin does not show up in the Cs isotopes in the present calculation. This is because the radial wave functions of loosely bound proton orbits are damped strongly by the Coulomb barrier. Thus, for nuclei with larger Z, the proton skin formation is not very feasible, whereas it may be possible in nuclei with smaller Z, as seen in the above example of Al isotopes.

VIII. EFFECTS OF NEUTRON SKIN

The neutron skin is expected to have a prominent effect on nuclear reactions, for instance, fusion initiated by neutron flow [12,13]. If an unstable nucleus with the neutron skin approaches a stable nucleus, neutrons in the skin can touch the other nucleus before protons can do so, since those neutrons are distributed outside protons. Since the Fermi energy is so different between the two nuclei, neutrons in the skin may flow into the stable nucleus while the two nuclei are touching nearly at rest in their relative motion. Note that neutrons in the skin are expected to have more mobility than neutrons in normal nuclei, because (i) a more gradual potential near the surface yields less reflection of incoming waves and, (ii) a mean free path of a neutron can be longer due to lower density. The soft dipole mode [9,14] is expected to occur in nuclei with the neutron skin. This mode may enhance the neutron flow, because the skin neutrons can be closer to the other nucleus while the protons are pushed away by the Coulomb repulsion. Combining the above effects, one can expect that such fast flow of neutrons, which can be viewed as "neutron avalanche," should occur, enhancing the reaction cross section. This will be an intriguing subject of future experiments with radioactive nuclear beams.

It is quite likely that the neutron skin should affect nuclear deformation, dynamic or static, in general. We shall consider here the restoring force against the surface deformation, which should be directly influenced by the neutron skin because the neutron surface is shifted outward compared to the proton surface. Neutrons excited from the skin should feel weaker restoring force due to the absence of protons in the neutron skin. This leads us to a mode comprised primarily of neutron particle-hole excitations only, referred to as the "neutron mode" later. The situation should be more complex for protons, because there are two opposite changes of the restoring force. The first one is its weakening; the binding from neutrons is less affected by a proton surface distortion, resulting in weaker restoring force. The enlargement of the radius of the proton potential also causes a lowering of energies of particle-hole excitations. However, the restoring force is made stronger due to deeper proton potential. To be more precise, when the potential becomes deeper, higher orbits gain less binding energy, because wave functions of these orbits extend outwards compared with more tightly bound orbits. The kinetic energy is also increased for higher but bound orbits due to tighter confinement. Thus, both the potential and kinetic terms tend to shift the excitation energies of the proton surface oscillations higher due to the deepening of the potential. Because of the above-mentioned opposite effects, the net effects may be rather small for protons.

One can expect from the above discussions that giant resonances with various multipolarities should be affected, similarly to the giant electric dipole and magnetic dipole resonances studied in Ref. [15]. Because the surface oscillation of protons and that of neutrons couple weakly in comparison with stable nuclei, the separation into the isoscalar and isovector giant resonances may be changed. This may result in (i) the increase of the energy of the isoscalar peak in comparison to stable nuclei of the same mass and (ii) the appearance of "neutron modes" even below the isoscalar peak due to weaker restoring force, being decoupled from proton excitations.

Another point of interest is the isobaric analog resonance built on a neutron-skin nucleus, because of the difference between U_p and U_n, large $\epsilon_p^{(F)}-\epsilon_n^{(F)}$, etc. The neutron skin thus opens up new fields of interest, which are presently being studied.

IX. RELATION TO NEUTRON HALO

We comment on the relation between the neutron skin and the neutron halo. They should be distinguished. The neutron skin is a phenomenon which involves rather many neutrons with relatively high density, whereas the neutron halo is caused by one or two neutrons extremely loosely bound with tremendously stretched distribution. The neutron halo is considered as a pure tunneling effect occurring probably only for the s ($l=0$) and p ($l=1$) orbits because of the centrifugal barrier. The neutron skin can occur in any orbit, and is formed in the radial region where the potential energy becomes about equal to the energies of several highest single-particle orbits. Thus, the tunneling is only an aspect of the neutron-skin formation. The typical density of neutrons in the neutron halo is less than $\frac{1}{100}$ of the central density as mentioned already [9]. Thus, the neutron skin can be distinguished from the halo, particularly in the definition introduced in the present paper, and the skin is, in comparison to the halo, more "macroscopic" and more bound with less extension. On the other hand, the neutron halo and skin may have some overlapping region.

X. SUMMARY

In summary, we have discussed the definition and appearance of the neutron skin in terms of the spherical Hartree-Fock calculation. We predicted the neutron skin in nuclei far from the β stability line. The proposed criteria preclude the neutron skin in stable nuclei, even with large neutron excess. The effects of deformation on the skin formation have not been investigated so far with our definition. They are expected rather minor, because of the general mechanism leading to the neutron skin. More details of the deformation effects should be further studied. The proton skin may be obtained as well in nuclei with $Z \gg N$, if Z is not too large. Several intriguing features expected from the neutron skin formation are

suggested, concerning the nuclear reaction involving a skin nucleus, giant resonances from a skin nucleus, etc.

ACKNOWLEDGMENTS

We are grateful to Dr. W. Bentz for careful reading of the manuscript. This work was supported in part by Grant-in-Aid for General Scientific Research (No. 04804012) by the Ministry of Education, Science and Culture. A part of this work was also supported by the Special Researchers' Basic Science Program at RIKEN. Numerical calculations were carried out at Meson Science Laboratory, the University of Tokyo and at RIKEN.

[1] A. Krasznahorkay *et al.*, Phys. Rev. Lett. **66**, 1287 (1991).
[2] W. D. Myers, W. J. Swiatecki, and C. S. Wang, Nucl. Phys. **A436**, 185 (1985).
[3] I. Tanihata, D. Hirata, T. Kobayashi, S. Shimoura, K. Sugimoto, and H. Toki, Phys. Lett. B **289**, 261 (1992).
[4] D. Vautherin and D. M. Brink, Phys. Rev. C **5**, 626 (1972).
[5] D. Vautherin, Phys. Rev. C **7**, 296 (1973).
[6] M. Beiner, H. Flocard, N. Van Giai, and P. Quentin, Nucl. Phys. **A238**, 29 (1975).
[7] N. Van Giai and H. Sagawa, Phys. Lett. **106B**, 379 (1981).
[8] A. Bohr and B. R. Mottelson, *Nuclear Structure* (Benjamin, Reading, MA, 1969), Vol. 1, p. 170.
[9] I. Tanihata, Nucl. Phys. **A522**, 275c (1991), and references therein.
[10] C. B. Dover and N. Van Giai, Nucl. Phys. **A190**, 373 (1972).
[11] E. W. Otten, in *Treatise on Heavy-Ion Science,* Vol. 8 of *Nuclei Far from Stability,* edited by D. A. Bromley (Plenum, New York, 1989).
[12] P. H. Stelson, Phys. Lett. **B205**, 190 (1988).
[13] P. H. Stelson, H. J. Kim, M. Beckerman, D. Shapira, and R. L. Robinson, Phys. Rev. C **41**, 1584 (1990).
[14] K. Ikeda, Nucl. Phys. **A538**, 355c (1992).
[15] P. Van Isacker, M. A. Nagarajan, and D. D. Warner, Phys. Rev. C **45**, R13 (1992).